EDGEWOOD CHEMICAL BIOLOGICAL CENTER
U.S. ARMY RESEARCH, DEVELOPMENT AND ENGINEERING COMMAND
Aberdeen Proving Ground, MD 21010-5424

ECBC-TR-1512

RAMAN SPECTRA AND CROSS SECTIONS OF CHEMICAL WARFARE AGENTS, AGENT SIMULANTS, AND EXPLOSIVES USING 213 NM DEEP-ULTRAVIOLET LASER EXCITATION

Phillip G. Wilcox
Erik D. Emmons
Ian J. Pardoe

RESEARCH AND TECHNOLOGY DIRECTORATE

May 2018

U.S. ARMY RDECOM

Disclaimer

The findings in this report are not to be construed as an official
Department of the Army position unless so designated by other authorizing documents.

REPORT DOCUMENTATION PAGE

Form Approved
OMB No. 0704-0188

1. REPORT DATE *(DD-MM-YYYY)*	**2. REPORT TYPE**	**3. DATES COVERED** *(From - To)*
XX-05-2018	Final	May 2016–Jan 2018

4. TITLE AND SUBTITLE
Raman Spectra and Cross Sections of Chemical Warfare Agents, Agent Simulants, and Explosives Using 213 nm Deep-Ultraviolet Laser Excitation

5a. CONTRACT NUMBER

5b. GRANT NUMBER

5c. PROGRAM ELEMENT NUMBER

6. AUTHOR(S)
Wilcox, Phillip G.; Emmons, Erik D.; and Pardoe, Ian J.

5d. PROJECT NUMBER
CB10056

5e. TASK NUMBER

5f. WORK UNIT NUMBER

7. PERFORMING ORGANIZATION NAME(S) AND ADDRESS(ES)
Director, ECBC, ATTN: RDCB-DRI-S, APG, MD 21010-5424

8. PERFORMING ORGANIZATION REPORT NUMBER
ECBC-TR-1512

9. SPONSORING / MONITORING AGENCY NAME(S) AND ADDRESS(ES)

10. SPONSOR/MONITOR'S ACRONYM(S)

11. SPONSOR/MONITOR'S REPORT NUMBER(S)

12. DISTRIBUTION / AVAILABILITY STATEMENT
Approved for public release: distribution unlimited.

13. SUPPLEMENTARY NOTES

14. ABSTRACT-LIMIT 200 WORDS

A solid-state, deep-ultraviolet (DUV) laser operating at 213 nm was procured under the Foreign Technology Assessment Support (FTAS) program. The laser was characterized and integrated into a Raman test fixture to assess the laser's applicability for DUV resonance Raman spectroscopy. Under the FTAS program and a similar effort from the Joint Science and Technology Office of the Defense Threat Reduction Agency, this test bed was used to collect 213 nm Raman spectra for chemical warfare agents (CWAs), CWA simulants, and exposive materials and precursors. Raman cross sections were calculated for the CWAs and CWA simulants. Finally, an analysis was performed using previous DUV Raman cross sections to determine the trade-offs between the Raman scattering enhancement that occurs using shorter excitation sources and the signal reduction caused by higher optical absorption.

15. SUBJECT TERMS

Raman spectroscopy	213 nm Raman	Deep ultraviolet (DUV)	Simulant
Raman cross section	Chemical warfare agent (CWA)	Resonance Raman	Explosive

16. SECURITY CLASSIFICATION OF:			**17. LIMITATION OF ABSTRACT**	**18. NUMBER OF PAGES**	**19a. NAME OF RESPONSIBLE PERSON**
a. REPORT	**b. ABSTRACT**	**c. THIS PAGE**			Renu B. Rastogi
U	U	U	UU	32	**19b. TELEPHONE NUMBER** *(include area code)* (410) 436-7545

Standard Form 298 (Rev. 8-98)
Prescribed by ANSI Std. Z39.18

Blank

PREFACE

The work described in this report was authorized under the Foreign Technology Assessment Support program and the Defense Threat Reduction Agency Joint Science and Technology Office's Chemical Early Warning project no. CB10056. The work was started in May 2016 and completed in January 2018.

The use of either trade or manufacturers' names in this report does not constitute an official endorsement of any commercial products. This report may not be cited for purposes of advertisement.

This report has been approved for public release.

Blank

CONTENTS

FIGURES

TABLES

RAMAN SPECTRA AND CROSS SECTIONS OF CHEMICAL WARFARE AGENTS, AGENT SIMULANTS, AND EXPLOSIVES USING 213 NM DEEP-ULTRAVIOLET LASER EXCITATION

1. INTRODUCTION

Raman spectroscopy is an analytical technique that uses light scattered from a monochromatic laser to detect and identify chemicals. The laser light is used to excite molecular vibrations. These vibrations cause some inelastically scattered incident photons to return to the detector at different wavelengths creating a unique fingerprint that corresponds to a unique molecular structure that can be used for chemical identification. Commercially available instruments based on this technique are currently used by military units such as the 20th Chemical, Biological, Radiological, Nuclear, and Explosives (CBRNE) Command and civilian first responders. Raman spectroscopy has benefits over other analytical techniques: it is fast (measurements can be done in seconds), it requires no sample preparation or consumables, it may allow measurement without physical contact with the sample, and it is nondestructive, which allows for samples to be saved and further investigated using more sensitive and/or orthogonal techniques. As laser and detector technologies have improved, the size of Raman instruments has shrunk to where small, handheld units are available from multiple vendors. However, these instruments have very short standoff ranges (~1 cm) that require the system to be placed directly against or in very close proximity to the unknown samples. Proximal Raman systems (which have standoff distances from 10 cm to 200 m) are an active area of research (*1*). These proximal instruments allow soldiers and first responders to identify chemical threats from farther away, which increases the individuals' safety and reduces the sampling burden.

The most common types of commercial Raman sensors use visible or near-infrared (NIR) excitation due to the wide availability of high-power, narrow-line-width lasers in these wavelength regions. Moving to the shorter excitation wavelengths of deep-ultraviolet (DUV) Raman spectroscopy, which uses laser wavelengths of <250 nm, is desirable to improve both the Raman signal strength and the ability to detect. Operating in this wavelength range reduces the influence of interfering signals from solar radiation and sample fluorescence. Fluorescence occurs when an electronic state of the analyte is excited and re-emits light of different wavelengths. This can be a very strong process, and the broadband light that is emitted can overwhelm the Raman scattered light. Raman scattering is a relatively weak phenomenon; often, the probability of a photon generating Raman scatter, which is proportional to a measurable value known as the Raman cross section, can be in the range of 10^{-6} to 10^{-8}. UV light excitation can be more desirable than NIR or visible light excitation because the Raman cross section is proportional to $1/\lambda^4$, which provides a significant boost in Raman return signal strength. Furthermore, UV excitation increases the chance that resonance Raman enhancement will occur, whereby the wavelength of the excitation light overlaps with an electronic transition of the molecule. This process results in a very rapid increase (up to several orders of magnitude) in the cross section of the analyte molecule.

The drawback to DUV Raman spectroscopy is that laser sources at this wavelength are typically either laboratory-size instruments or small, low-power systems, neither of which is suitable for portable Raman systems. Examples include continuous-wave (CW) frequency-doubled argon ion lasers, which emit several discrete lines in the range of 229–257 nm. These lasers require liquid cooling and >10 kW of electronic power input to produce <1 W of UV light; therefore, they are not feasible for field use. Another example is the KrF excimer laser, which emits at 248 nm. These lasers are low-repetition-rate, high-pulse-energy systems that can cause sample damage. In addition, they suffer from reliability issues: under exposure to even trace atmospheric contamination, the KrF gas rapidly degrades. Smaller lasers exist, such as NeCu and HeAg lasers, which output at 248.6 and 224.3 nm, respectively. These systems are small enough to be integrated into handheld systems, but their output is <0.5 mW.

Under the Foreign Technology Assessment Support (FTAS) program, members of the U.S. Army Edgewood Chemical Biological Center (ECBC) Spectroscopy Branch were able to procure and characterize a 213 nm diode pumped, high-repetition-rate, Q-switched UV laser called the Impress 213, which was designed and manufactured by Xiton Photonics GmbH (Kaisserslautern, Germany). This system has an advantage over other DUV systems in that it runs at high repetition rates (on the order of 10 kHz) with relatively low pulse energies, to produce moderately high average power (up to 150 mW). These systems are sometimes denoted as quasi-CW systems because in practice, their mode of operation is similar to that of CW lasers. This operational advantage results in minimal damage to the samples. Similar systems have been available at 262 and 266 nm, but these wavelengths are above the 250 nm target, where fluorescence and solar radiation can cause sample interference. Until now, a laser of this type with a wavelength of <250 nm has been unavailable. After the laser was characterized, it was integrated into a Raman spectroscopic configuration and used to collect Raman signatures of explosives and chemical warfare agent (CWA) simulants. The Defense Threat Reduction Agency, Joint Science and Technology Office (DTRA JSTO) provided additional funding under the Chemical Early Warning project to measure surety CWAs and calculate the Raman cross sections using this system. This work supports better understanding of the UV resonance enhancement using 213 nm laser excitation as well as quantification of the trade-offs caused by higher self-absorption from the chemical of interest.

2. LASER CHARACTERIZATION

2.1 System Description

The Impress 213 from Xiton Photonics is a frequency-quintupled, neodymium-doped yttrium–aluminium–garnet (Nd:YAG) laser that operates at 213 nm. The laser system is shown in Figure 1 and consists of three main components: a laser head, a power supply, and a chiller. The laser head is approximately 15.5 × 12.6 × 3.8 in. The model procured by the ECBC team had an added 3.5 × 7.3 × 3.8 in. module attached to the laser head to allow for the addition of a shutter and notification lights. This addition was necessary for compliance with safety requirements from the Food and Drug Administration’s Center for Devices and Radiological Health (CDRH) before the system was imported into the United States. This CDRH module is required for laser use on a laboratory benchtop, but it would not be required if the laser were

contained within a larger instrument system, which would render the laser safe by containment. The power supply and chiller are both 3U rack-mountable units. The power supply is approximately 17.5 × 17.5 × 5.25 in., and the chiller is approximately 15 × 17.5 × 5.25 in.

The laser was controlled via an external computer using RS-232 communication. The laser contains three nonlinear optical (NLO) crystals that must heat up and be tuned before use, which can take 1–2 h from a cold start. During operation, the laser head requires a nitrogen purge to keep the crystals dry and clean. Before the system is shut down completely, it must perform a controlled cool-down of the crystals, which can also take 1–2 h.

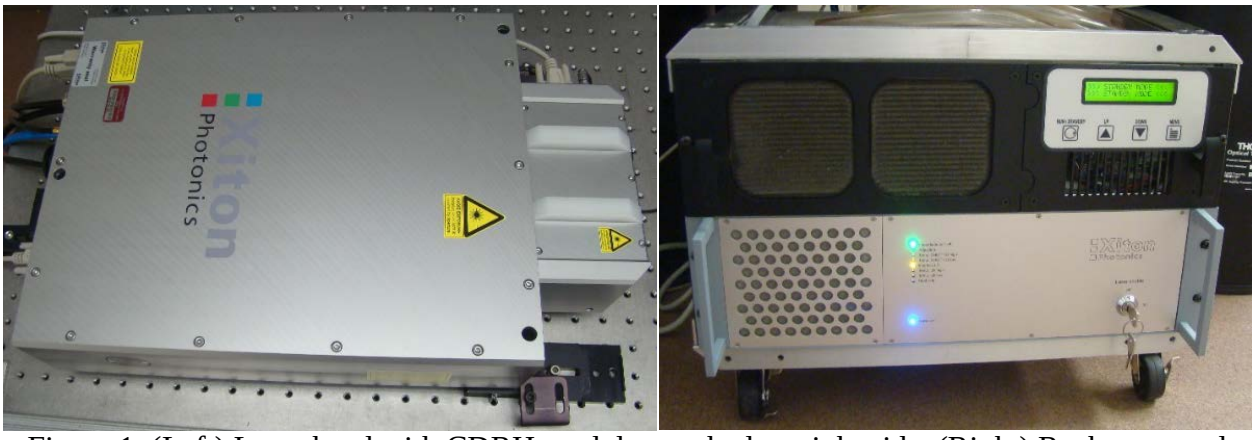

Figure 1. (Left) Laser head with CDRH module attached on right side. (Right) Rack-mounted chiller (top) and power supply (bottom).

2.2 Output Power

The maximum output power for the system was measured to be approximately 150 mW; however, users can control the output power. Theoretically, the power could be increased beyond 150 mW by increasing the power on the laser diode that is used to pump the Nd:YAG crystal. Because these higher powers would more rapidly degrade the NLO crystals, they were not tested. With regular use, the NLO crystals will degrade over time even at 150 mW. The system includes a mechanical *x*–*y* stage that repositions the crystal and allows the laser to pass through undamaged portions. Xiton personnel provided *x*–*y* coordinates for 25 crystal locations that can be used to generate 213 nm light. No output degradation was noticed during the course of our experiments.

To measure the power stability, the laser was set up to operate for >5 h, and measurements were obtained every 0.17 s. As the laser operates, the NLO crystals heat up. This can affect the conversion efficiency and reduce the output power. However, the power decrease that occurred during our experiment was minimal, as shown in Figure 2.

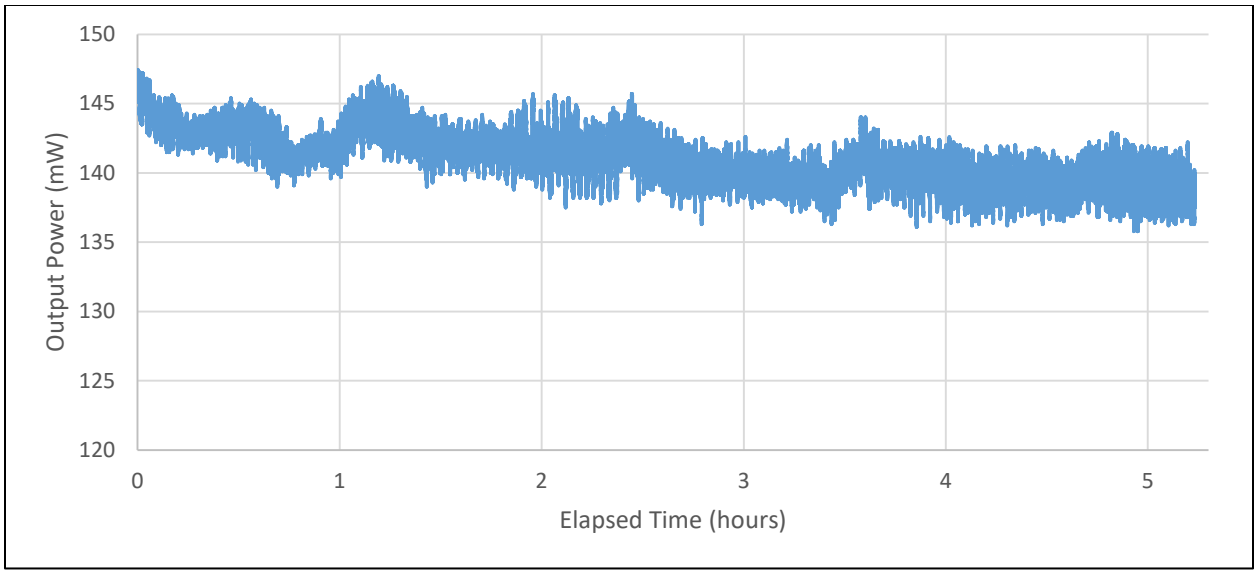

Figure 2. Output power measured over time (laser operating at 12.5 kHz).

Additionally, the system includes an internal attenuator that allows the output power to be controlled via external software. Figure 3 shows an example of how the output power can be controlled using the attenuator while the laser is operated at 12.5 kHz.

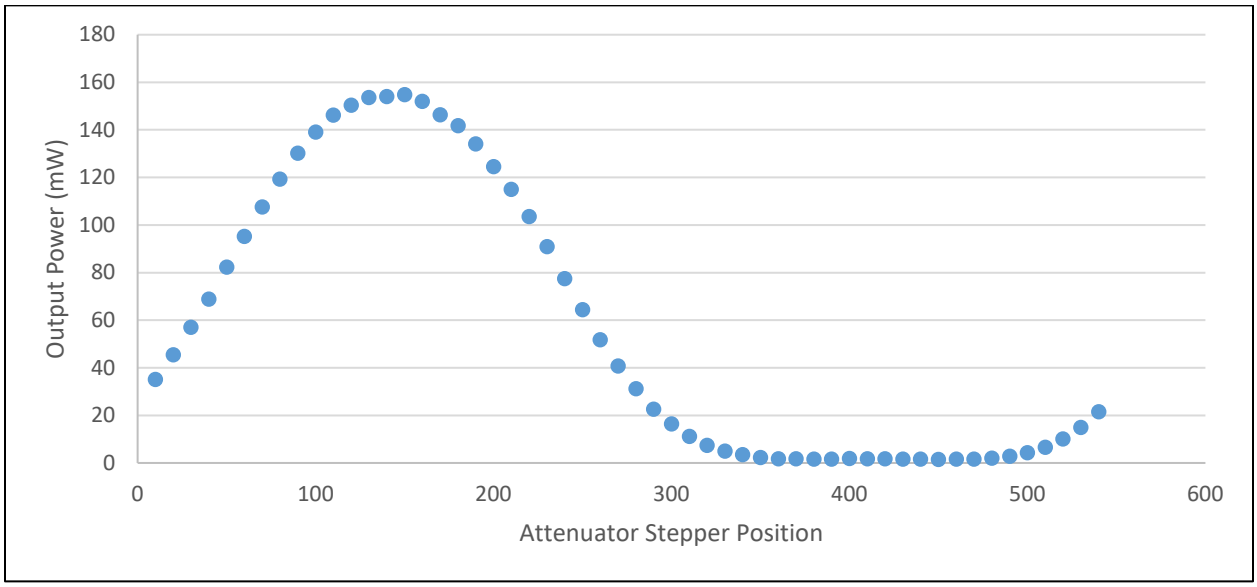

Figure 3. Control of the output power using the internal attenuator (laser operating at 12.5 kHz).

The repetition rate of the laser can also be controlled using the software, which affects the output power. Figure 4 shows how the average output power and the energy per pulse are affected when the repetition rate is varied.

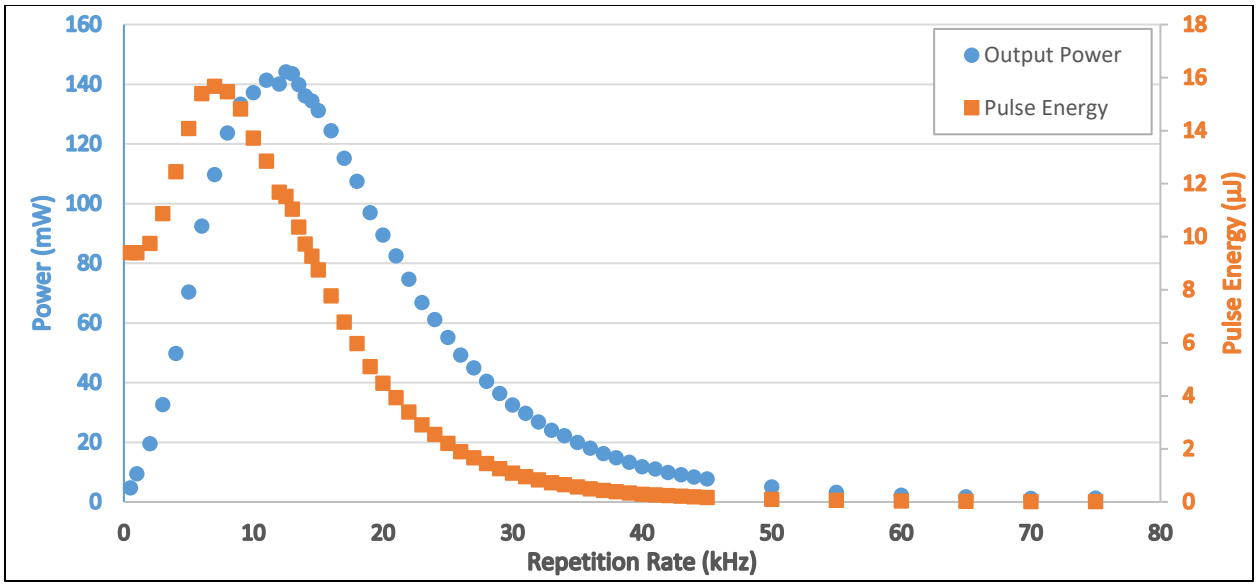

Figure 4. Effect of repetition rate on output power and pulse energy.

2.3 Beam Profile

A laser's beam profile is an important characteristic that indicates how tightly the laser can be focused and how well it can be coupled with optical components such as fiber optics or NLO crystals. The Xiton specifications indicate that the laser has a beam quality factor (M^2) of <1.6, and discussions with the company revealed that the M^2 is typically closer to 1.2–1.3. ECBC workers did not measure the M^2 to validate the vendor's claims, but the beam profile in Figure 5 shows a tight Gaussian beam that is consistent with these values.

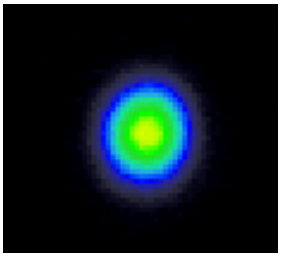

Figure 5. Measured beam profile of Xiton laser.

3. RAMAN MEASUREMENTS

The Xiton laser was integrated with collection optics, an optical filter, and a spectrometer (detailed in Section 3.1) to collect Raman signatures from a variety of chemicals. The data collection detailed in this report was performed under two separate efforts. The first was for DTRA JSTO, which provided funding to measure Raman cross sections for the CWAs and CWA simulants listed in Table 1. During the second effort, for FTAS, Raman signatures of the energetic materials listed in Table 2 were measured.

Table 1. List of CWAs and CWA Simulants Measured for Cross-Section Calculations Using 213 nm Raman Excitation

Chemical Name	CAS No.	Description
Cyclosarin (GF)	329-99-7	CWA, nerve
Diisopropyl methylphosphonate (DIMP)	1445-75-6	CWA simulant, nerve
Dimethyl methylphosphonate (DMMP)	756-79-6	CWA simulant, nerve
Methylphosphonic acid (MPA)	993-13-5	Solid CWA simulant, nerve
Methyl salicylate (MES)	119-36-8	CWA simulant, nerve
Sarin (GB)	107-44-8	CWA, nerve
Soman (GD)	96-64-0	CWA, nerve
Sulfur mustard (HD)	505-60-2	CWA, blister
Tabun (GA)	77-81-6	CWA, nerve
Thiodiglycol (TDG)	111-48-8	CWA simulant, blister
Triethyl phosphate (TEPO)	78-40-0	CWA simulant, nerve
VX	50782-69-9	CWA, nerve

Table 2. List of Energetic Materials Measured Using 213 nm Raman Excitation

Chemical Name	CAS No.	Description
2,4-Dinitrotoluene (2,4-DNT)	121-14-2	Explosive precursor
2,6-Dinitrotoluene (2,6-DNT)	606-20-2	Explosive precursor
Ammonium nitrate	6484-52-2	Explosive
Ammonium perchlorate	7790-98-9	Explosive precursor
Ammonium sulfate	7783-20-2	Explosive precursor
HMX	2691-41-0	Explosive
Pentaerythritol tetranitrate (PETN)	78-11-5	Explosive
Potassium perchlorate	7778-74-7	Explosive precursor
Potassium nitrate	7757-79-1	Explosive precursor
RDX	121-82-4	Explosive
Trinitrotoluene (TNT)	118-96-7	Explosive

3.1 System Configuration

The laser, operating at 30 mW output power, was integrated into two different Raman configurations. The first was in a general-use laboratory to collect spectra from the explosives and the CWA simulants. The second was located in a chemical surety laboratory to collect data on the CWAs. The two setups were similar, and each included an Edmund Optics (Barrington, NJ) infinite-conjugate, DUV-coated aluminum, reflective 15× objective lens to collect the Raman scattered light at approximately 1 in. from the sample. The Rayleigh line (the resultant from the elastic backscatter of incident photons, which is much stronger than Raman scatter) was filtered out using a custom 213 edge filter from Optics Balzers (Jena, Germany). Edge filters at this wavelength are difficult to manufacture; the short wavelength reduces the spacing in wavenumber (in inverse centimeters) space. This means that the transition between the high optical density region to block the Rayleigh scatter and the bandpass to allow the Raman return has tighter tolerance than occurs in the visible or NIR regions. Because of this, the Raman

system was unable to collect signals below ~700 cm^{-1}, as shown in the filter-transmission profile in Figure 6. The Raman light was collected in a Princeton Instruments (Acton, MA) Acton SP-2500 spectrometer using a 2400 lines/mm grating and a Princeton Instruments Pixis 2K camera. The main difference between the two configurations is that in the non-surety configuration, collected light is transmitted through free-space optics, whereas in the surety configuration, it is transferred through an optical fiber. Propagation though a fiber optic introduces loss that may be non-uniform across the spectrum. A broadband DH-2000-CAL deuterium calibration lamp (Ocean Optics; Largo, FL) was used to correct the intensity of all data in this effort and thereby negate this effect in the final results.

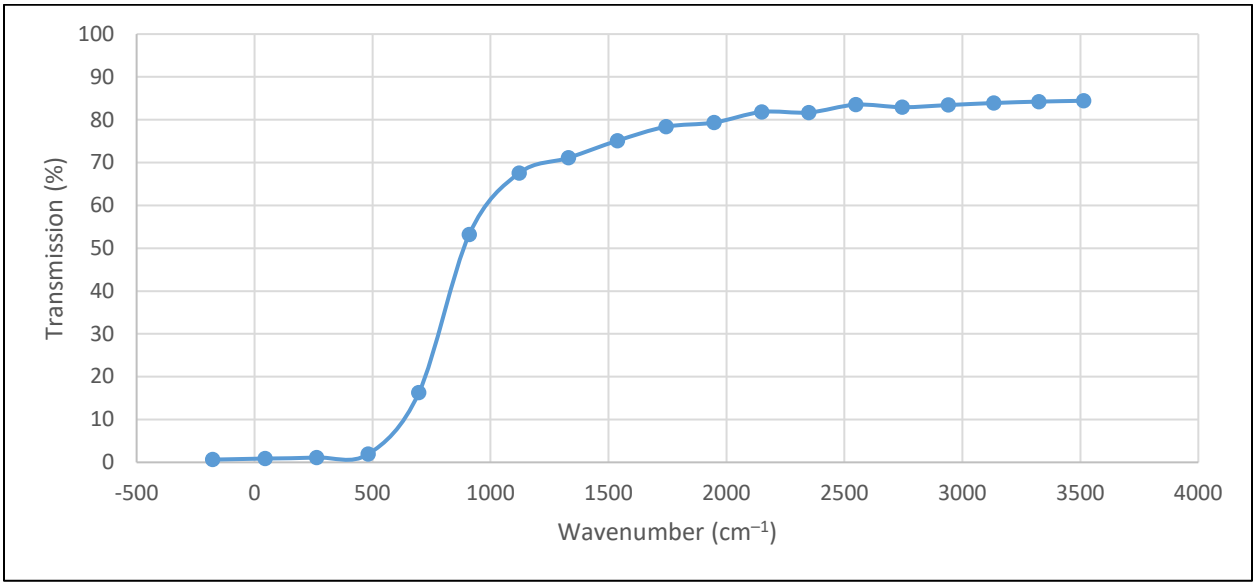

Figure 6. Transmission profile of custom 213 nm edge filter manufactured by Optics Balzers.

3.2 Raman Cross-Section Calculations

Direct calculation of the Raman cross section is very complex and hard to achieve for even small- to mid-sized molecules. Because of this, we used an internal standard method whereby the agent scattering intensities were compared with those of a known standard, acetonitrile. Acetonitrile was chosen as an internal reference because its cross-sectional value is well established for UV wavelength excitation (*2*, *3*), and it has a UV absorption cutoff wavelength (10% transmission through 1 cm path) of 190 nm (*4*). The samples were mixed with acetonitrile in concentrations ranging from approximately 5 to 75% of analyte by volume, and approximately 300 µL of this solution was pipetted into a glass sample cup for analysis. A magnetic stir bar was used during data collection to counteract potential photodegradation of the sample by the laser.

For these measurements, we used the values for the Albrecht A-term fit parameters reported by Dudik et al. (*2*) to calculate the Raman cross sections of the acetonitrile bands at 918 and 2249 cm^{-1} at 213 nm to use as our internal standard. The Raman scattering

cross sections are determined by a comparison of the integrated line intensity (integrated area) of a Raman band of the sample with that of the acetonitrile:

$$\sigma_R^s = \sigma_R^r \left(\frac{I^s}{I^r}\right)\left[\frac{E\left(\nu_o - \nu_j^r\right)}{E\left(\nu_o - \nu_j^s\right)}\right]\left(\frac{C^r}{C^s}\right) \quad (1)$$

where σ_R is the Raman cross section;

I is the integrated area of the Raman band;

$E(\nu_o - \nu_j)$ is the spectrometer efficiency at the Raman frequency at the specified Raman shifted frequency of $\nu_o - \nu_j$ (all spectra were intensity-corrected using a calibrated DH-2000-CAL deuterium lamp to account for E);

superscripts r and s refer to the reference (acetonitrile) and sample (CWA or simulant), respectively; and

c is the sample concentration in molecules per unit volume.

3.3 Chemical Warfare Simulants and Agents

Under this effort, we were able to measure six CWAs and six CWA simulants using the 213 nm Raman system. All of the simulants were acquired commercially from Sigma-Aldrich (St. Louis, MO), and the CWAs were provided by the ECBC Agent Chemistry Branch. Of the 12 total chemicals, cross sections were successfully calculated for nine chemicals, and those values are listed in Table 3. The Raman signatures of HD and VX did not show any measureable Raman peaks, possibly because of rapid photodegradation caused by the UV light or absorption by impurities in the samples. For TDG, the main spectral feature was at approximately 654 cm^{-1}, which is below the cutoff of the filter. Raman spectra for the CWA simulants are shown in Figure 7, and the signatures for the CWAs are shown in Figure 8.

Table 3. Measured Raman Cross Sections Using 213 nm Laser Excitation

Chemical	Peak (cm^{-1})	Cross Section (cm^2/sr/molecule)
GA	2195	8.01×10^{-27}
GB	724	2.56×10^{-28}
GD	730 + 751	7.68×10^{-28}
GF	752	2.75×10^{-28}
HD	No peaks	
VX	No peaks	
DIMP	716	3.50×10^{-28}
DMMP	706 + 715	4.56×10^{-28}
MES	807	1.46×10^{-24}
MPA	774	4.75×10^{-28}
TDG	654	Filter cutoff
TEPO	730	4.43×10^{-28}

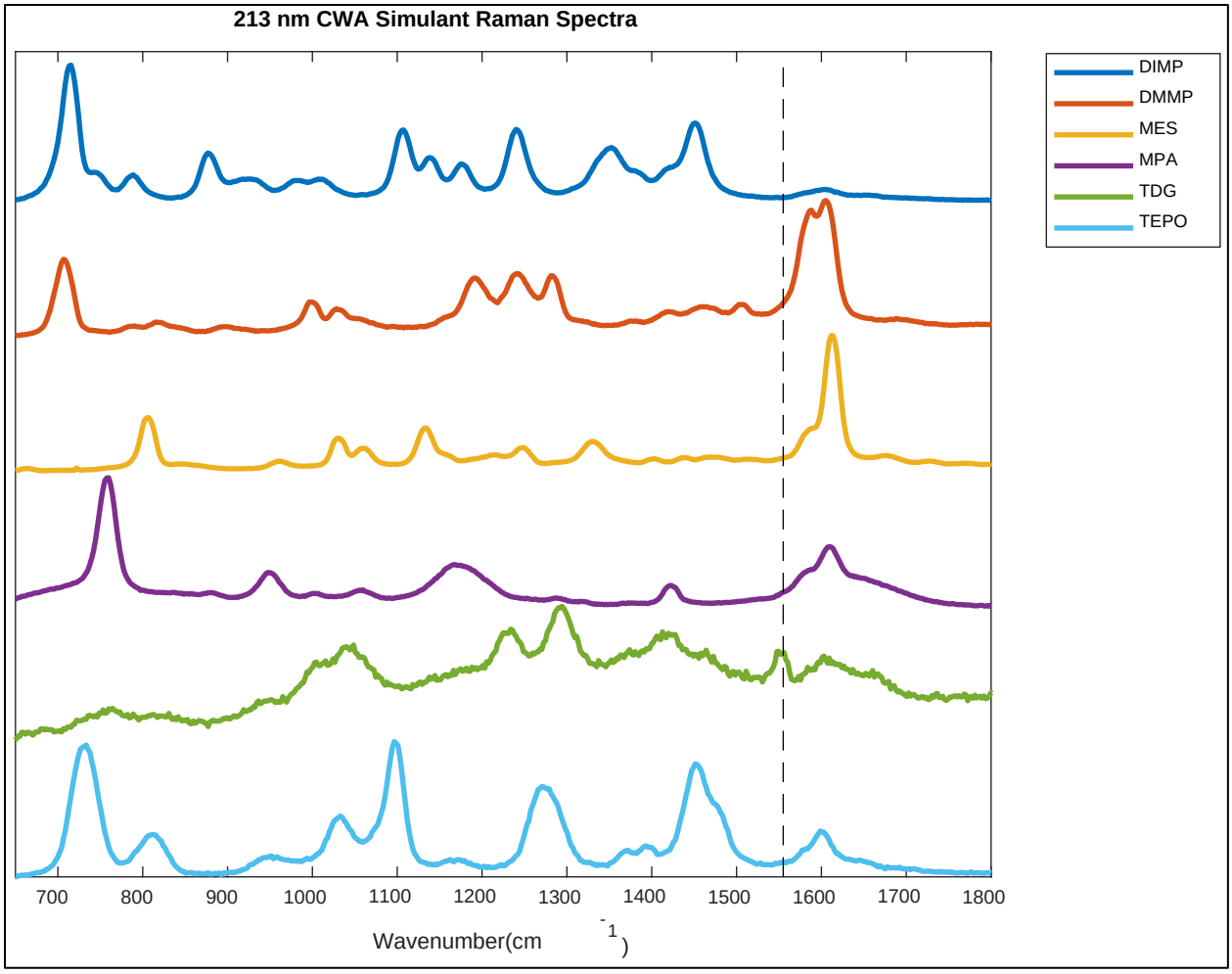

Figure 7. Raman spectra of CWA simulants collected using 213 nm laser excitation. Dashed line represents a peak attributed to atmospheric oxygen and not the CWA simulants.

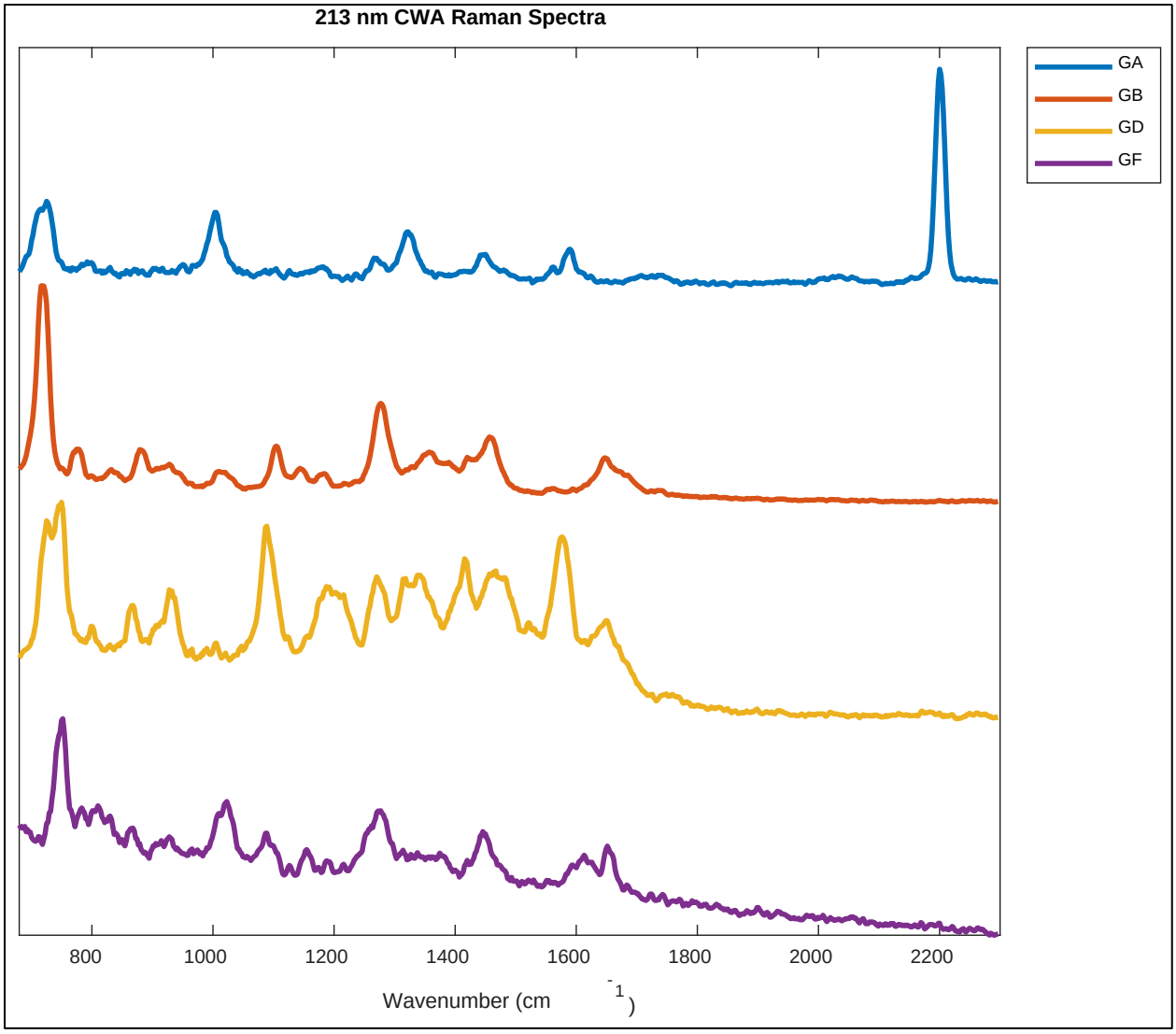

Figure 8. Raman spectra of CWAs collected using 213 nm laser excitation. HD and VX were also measured during this effort; however, no discernable peaks were present in the fingerprint region, so they were excluded from this figure.

3.4 Relative Raman Signal

To calculate the Raman scattering intensity of a given chemical, it is necessary to know how much of the incident scattered radiation is absorbed by the sample. For samples transparent at the relative wavelengths, the absorbance is negligible, and no correction is required. However, many organic chemicals have absorbance bands below 300 nm, and this absorbance must be taken into account when Raman scattering cross sections are calculated. The amount of radiation absorbed by a molecule is described by the Beer–Lambert law:

$$I = I_0 \times 10^{-\varepsilon c L} \quad (2)$$

where I_0 is the intensity of incident radiation,
I is the intensity of transmitted radiation,
c is the molar concentration (M),
L is the path length of the cell (cm), and
ε is the molar absorptivity or molar extinction coefficient (L/mol/cm).

The observed intensity of a given Raman line is proportional to the Raman scattering cross section and the number of molecules that contribute to that scattering. The latter term is a function of the molecular absorbance. The absorbance determines the depth of penetration by the laser excitation and the amount of Raman scattered light that is reabsorbed by the sample. The relative return Raman signal strength can be determined using

$$\text{Raman signal} \propto \sigma_R \times \rho \times \int_0^D 10^{-(\alpha_0+\alpha_R)r} \mathrm{d}r \quad (3)$$

where σ_R is the Raman cross section (cm^2/sr/molecule),
ρ is the density (molecules/cm^3),
D is the sample thickness (cm),
α_0 is the absorption cross section at the laser wavelength (cm^2/molecule), and
α_R is the absorption cross section at the Raman wavelength (cm^2/molecule).

Equation 3 can be used to calculate the relative signal strengths as a function of sample thickness and excitation wavelength. The equation assumes that the sample has a uniform depth and is at least as large as the extent of the laser spot. Figures 9–16 show the effect that sample thickness has on the return signals for GA, GB, GD, GF, DIMP, DMMP, MES, and TEPO. All of the Raman cross-sectional values that were used for these calculations were previously calculated at the ECBC Spectroscopy Branch. Most of these can be found in references *5* and *6*; however, some are unpublished. The molar absorptivity values were taken from reference *7*. Reference *7* only reports values out to 400 nm, so all absorbances longer than 400 nm were taken to be zero. It should be noted that for all seven of these plots, both the *x* and *y* axes are logarithmic.

All of the plots have the same general shape, with the return from 213 nm excitation the highest for thin samples. As the samples became thicker, the UV absorption of the sample became a factor that caused the signal strength to plateau. This allowed the longer-excitation Raman signals to cross over and become dominant. This crossover point was smallest for GD and GF at approximately 30 and 100 µm, respectively. The crossover point for GB and DIMP occurred around a 1000 µm thickness, whereas GA, DMMP, and TEPO did not cross over until a 10,000 µm thickness. MES had a molar absorptivity that was approximately 2 orders of magnitude greater than that for all of the other measured chemicals. Its plateau occurred for very thin samples (~0.7 µm); however, the strong Raman cross section in the UV meant that the 532 nm did not cross over until the sample thickness was around 10,000 µm.

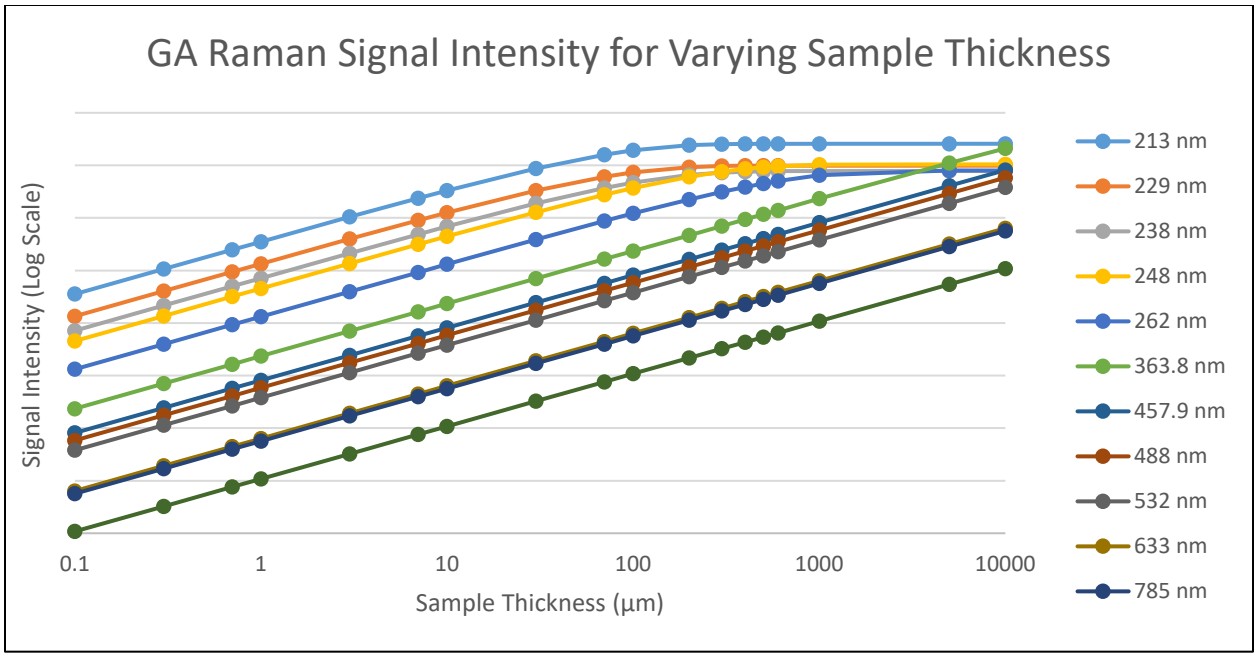

Figure 9. Relative Raman signal intensity for GA of varying sample thicknesses.

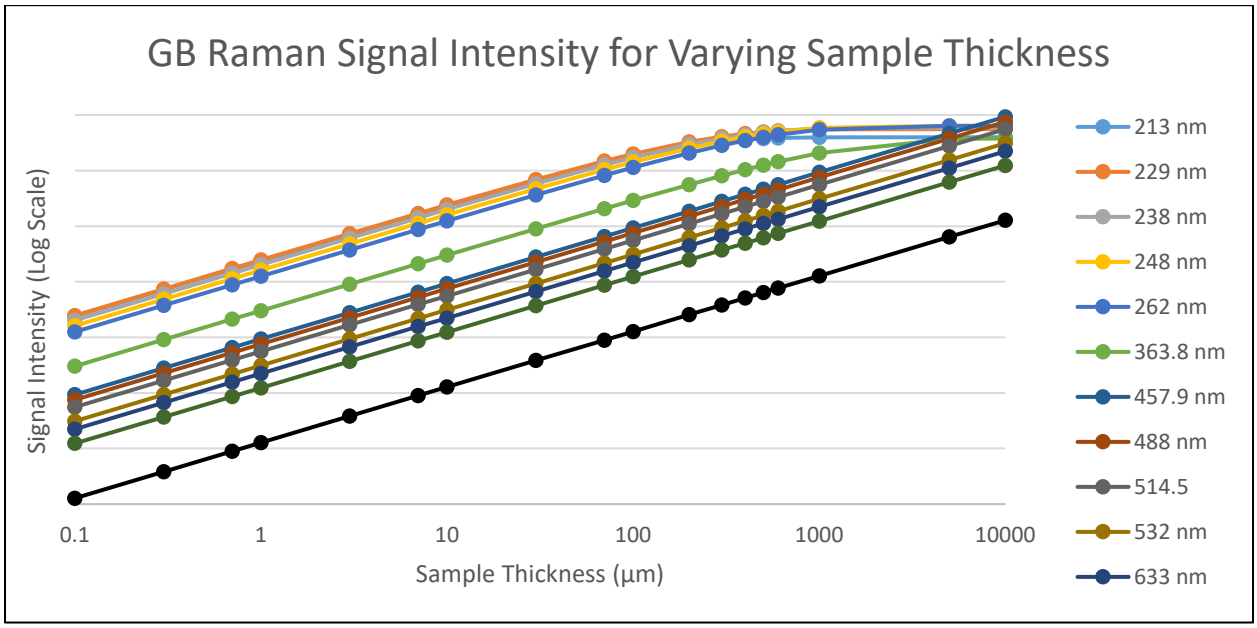

Figure 10. Relative Raman signal intensity for GB of varying sample thicknesses.

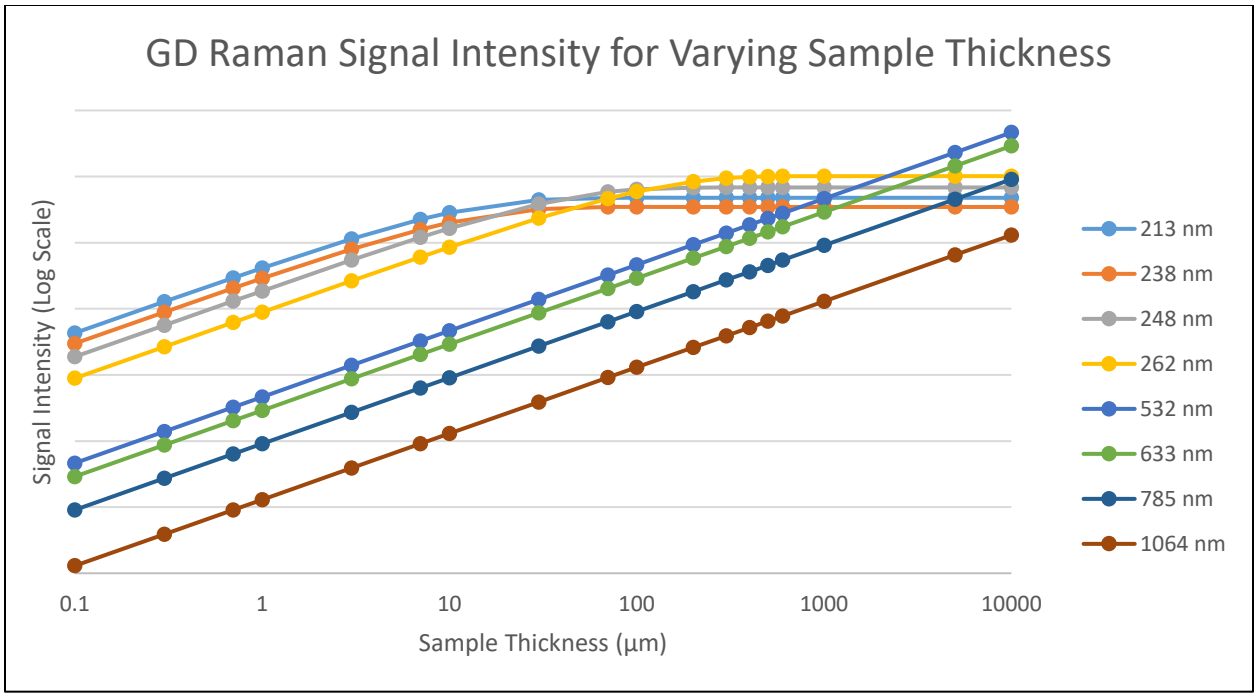

Figure 11. Relative Raman signal intensity for GD of varying sample thicknesses.

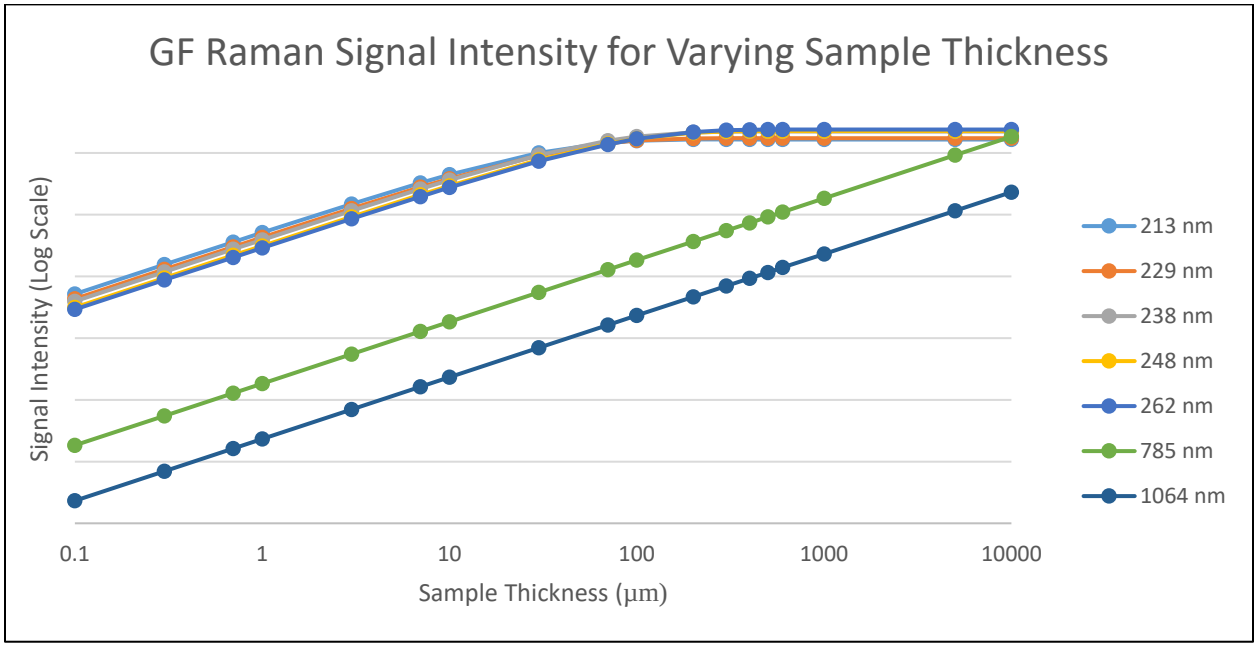

Figure 12. Relative Raman signal intensity for GF of varying sample thicknesses.

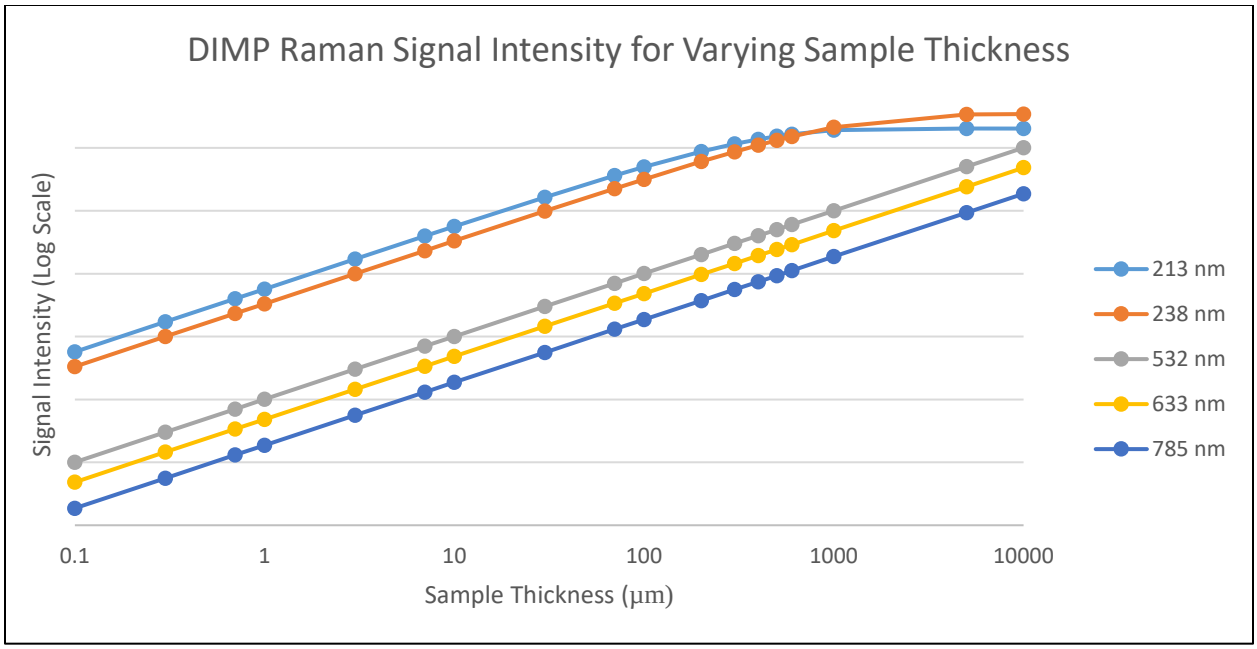

Figure 13. Relative Raman signal intensity for DIMP of varying sample thicknesses.

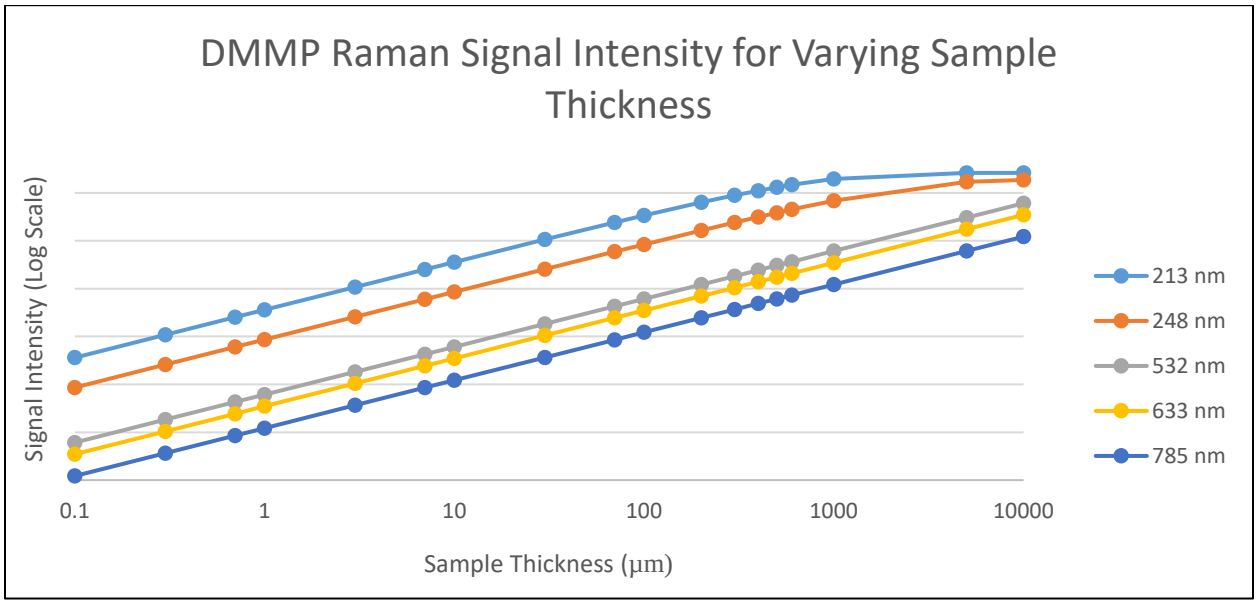

Figure 14. Relative Raman signal intensity for DMMP of varying sample thicknesses.

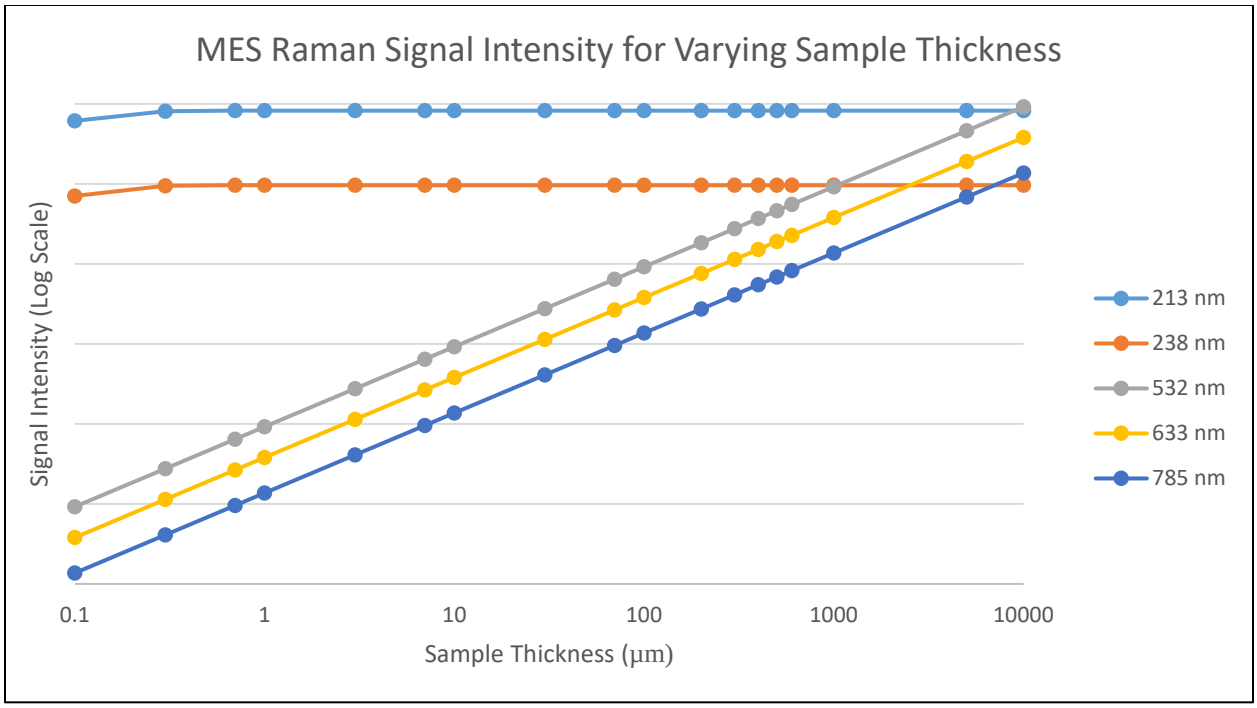

Figure 15. Relative Raman signal intensity for MES of varying sample thicknesses.

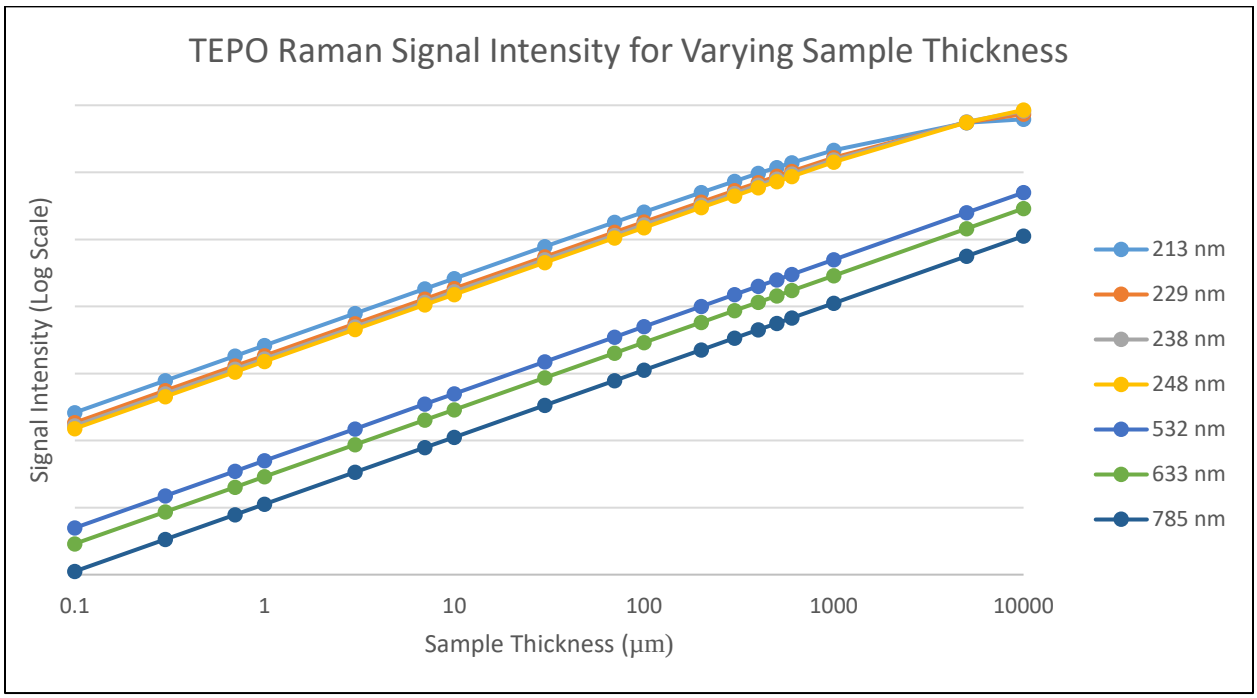

Figure 16. Relative Raman signal intensity for TEPO of varying sample thicknesses.

3.5 Explosives

Under this effort, Raman signatures from five high-explosive compounds and six explosive precursors were collected with 213 nm excitation and are shown in Figure 17. No cross-section calculations were performed with these chemicals; however, Raman peaks were visible and consistent with previous Raman measurements using other excitation wavelengths for all 11 compounds. This confirms the ability to use a 213 nm laser as an excitation source for detection and identification of these compounds through Raman spectra.

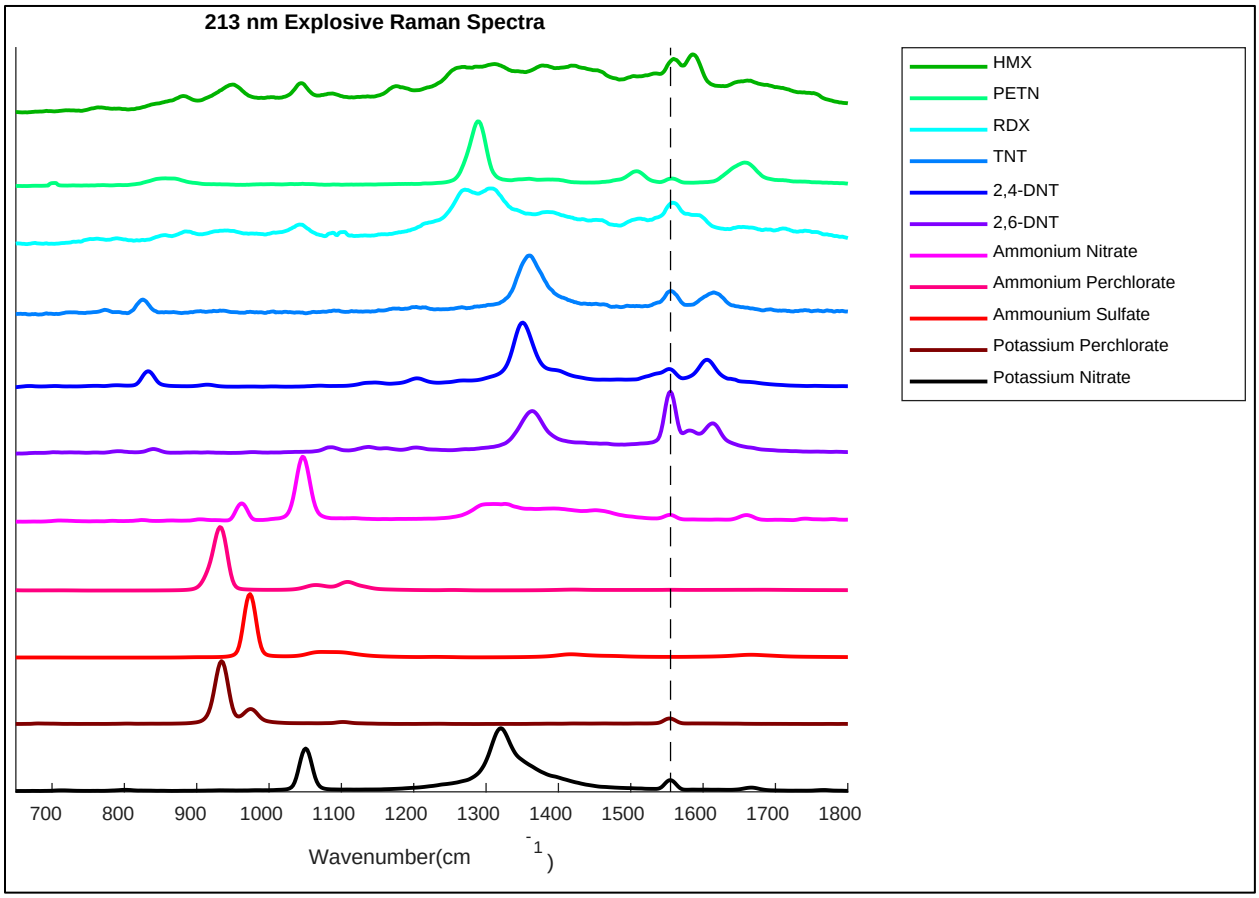

Figure 17. Raman spectra of explosive materials and precursors collected using 213 nm laser excitation. Dashed line represents a peak attributed to atmospheric oxygen and not to the explosive compounds.

4. CONCLUSION

In this effort, a Xiton 213 nm laser was used within a Raman spectroscopy setup to collect signatures from CWAs, CWA simulants, explosives, and explosive precursors. Signals could not be obtained from VX or HD, likely because of photodegradation, despite sample stirring. Also, due to limitations with the edge filter, low-wavenumber peaks (<700 cm^{-1}) were missed in the Raman fingerprint.

Quantitative Raman cross sections were calculated for CWAs and CWA simulants. Using these and previously obtained values, it was possible to model the expected Raman return for different sample types when different excitation lasers were applied. For all of the measured chemicals, the 213 nm excitation gave the strongest Raman return for thin samples.

The laser provides excellent data in the laboratory; however, in its current state, it is not suitable for portable or on-the-move use. The laser head, although smaller than that of comparable UV laser systems, is still 742 $in.^3$ in volume, and it requires a rack-mounted chiller and power supply to operate. When consulted on this issue, Xiton engineers said they believe they can simplify the laser operation by removing some features specific to laboratory usage, such as the tunable attenuator and the crystal moving components. They think this would decrease the size of the 213 nm laser head to 40–50% of its current size. This miniaturized system could be air-cooled, which would remove the need for one of the two 3U rack units. Xiton representatives estimated that this miniaturized laser, including the same power supply that was used with the current laser, could be procured for approximately $150,000 (as of July 2016). Although this miniaturized system would still be too large for handheld use, the removal of the water cooling would make it more appealing for vehicle-mounted applications. Additionally, the Xiton laser was designed to operate with a maximum output power of 150 mW; however, under this effort, all work was performed at 30 mW. The results obtained using this lower power may support future design changes to reduce the laser size, weight, and power consumption.

Blank

LITERATURE CITED

1. Guicheteau, J.; Christesen, S.D.; Tripathi, A.; Emmons, E.D.; Wilcox, P.G.; Emge, D.K.; Pardoe, I.J; Fountain, A.W. Proximal and Point Detection of Contaminated Surfaces Using Raman Spectroscopy. *Proceedings of SPIE 8189, Optics and Photonics for Counterterrorism and Crime Fighting VII; Optical Materials in Defence Systems Technology VIII; and Quantum-Physics-Based Information Security*, **2011,** 818902, doi 10.1117/12.899243.

2. Dudik, J.M.; Johnson, C.R.; Asher, S.A. Wavelength Dependence of the Preresonance Raman Cross Sections of CH_3CN, SO_4^{2-}, ClO_4^-, and NO_3^-. *J. Chem. Phys.* **1985,** *82* (4), 1732–1740.

3. Li, B.; Myers, A.B. Absolute Raman Cross Sections for Cyclohexane, Acetonitrile, and Water in the Far-Ultraviolet Region. *J. Phys. Chem.* **1990,** *94* (10), 4051–4054.

4. Gillam, A.E.; Stern, E.S.; Timmons, C.J. *Gillam and Stern's Introduction to Electronic Absorption Spectroscopy in Organic Chemistry*, 3rd ed.; Edward Arnold: London, 1970.

5. Christesen, S.D. Raman Cross Sections of Chemical Agents and Simulants. *Appl. Spectrosc.* **1988,** *42* (2), 318−321.

6. Christesen, S.D.; Pendell Jones, J.; Lochner, J.M.; Hyre, A.M. Ultraviolet Raman Spectra and Cross-Sections of the G-Series Nerve Agents. *Appl. Spectrosc.* **2008,** *62* (10), 1078−1083.

7. Lochner, J.M.; Hyre, A.M.; Christesen, S.D.; Gonser, K.R. *Quantitative UV Absorbance Spectra of Chemical Agents and Simulants*; ECBC-TR-611; U.S. Army Edgewood Chemical Biological Center: Aberdeen Proving Ground, MD, 2008; UNCLASSIFIED Report (ADA479956).

Blank

ACRONYMS AND ABBREVIATIONS

2,4-DNT	2,4-dinitrotoluene, explosive precursor
2,6-DNT	2,6-dinitrotoluene, explosive precursor
CBRNE	Chemical, Biological, Radiological, Nuclear, and Explosives
CDRH	Center for Devices and Radiological Health
CW	continuous wave
CWA	chemical warfare agent
DIMP	diisopropyl methylphosphonate, CWA nerve simulant
DMMP	dimethyl methylphosphonate, CWA nerve simulant
DTRA JSTO	Defense Threat Reduction Agency, Joint Science and Technology Office
DUV	deep-ultraviolet
ECBC	U.S. Army Edgewood Chemical Biological Center
FTAS	Foreign Technology Assessment Support
GA	tabun, CWA nerve agent
GB	sarin, CWA nerve agent
GD	soman, CWA nerve agent
GF	cyclosarin, CWA nerve agent
HD	sulfur mustard, CWA, blister agent
HMX	explosive compound
M^2	beam quality factor
MES	methyl salicylate, CWA nerve simulant
MPA	methylphosphonic acid, solid CWA nerve simulant
Nd:YAG	neodymium-doped yttrium–aluminium–garnet
NIR	near-infrared
NLO	nonlinear optical
PETN	pentaerythritol tetranitrate, explosive compound
RDX	explosive compound
TDG	thiodiglycol, CWA blister simulant
TEPO	triethyl phosphate, CWA nerve simulant
TNT	trinitrotoluene, explosive compound
UV	ultraviolet
VX	CWA nerve agent

DISTRIBUTION LIST

The following individuals and organizations were provided with one Adobe portable document format (pdf) electronic version of this report:

U.S. Army Edgewood Chemical
Biological Center (ECBC)
RDCB-DRI-S
ATTN: Wilcox, P.
Emmons, E.
Vanderbeek, R.
RDCB-DRC-P
ATTN: Pardoe, I.
Ellzy, M.

Defense Threat Reduction Agency
J9-CBS
ATTN: Cronce, D.
Esposito, A.

Office of the Chief Counsel
AMSRD-CC
ATTN: Upchurch, V.

Department of Homeland Security
RDCB-PI-CSAC
ATTN: Mearns, H.

G-3 History Office
U.S. Army RDECOM
ATTN: Smart, J.

ECBC Rock Island
RDCB-DES
ATTN: Lee, K.
RDCB-DEM
ATTN: Grodecki, J.

Defense Technical Information Center
ATTN: DTIC OA

ECBC Technical Library
RDCB-DRB-BL
ATTN: Foppiano, S.
Stein, J.


EDGEWOOD CHEMICAL BIOLOGICAL CENTER
A U.S. Army RDECOM Laboratory